Role of Induced Fields in Railguns

Paul J Cote*, Mark A. Johnson, and Krystyna Truszkowska
Benet Laboratories, US Army Research Engineering and Development Command
*Corresponding author: Benet Laboratories, 1 Buffington Street, Watervliet, NY 12189, pcote@pica.army.mil

Abstract: We provide an analysis of the nature of emfs induced during the operation of a railgun. The focus here is on the railguns, but the results are applicable to a broad range of similar distributed parameter problems. The main sources of induced emfs are current changes and armature motion. New perspectives are presented. It is shown, for example, that there is no true motional emf in railguns, and an alternative approach is offered in terms of localized flux creation. COMSOL modeling is used to illustrate the main concepts and consequences of induced emfs, and to validate the analyses. Experimental data provide added validation. The results offer insights into previously unexplained phenomena commonly observed in railgun tests.

Keywords: railguns, motional emf, induced fields, Faraday rule.

1. Introduction

The functions of the inductances in idealized (lumped-parameter) circuits associated with solid armature or plasma armature railguns are well understood. On the other hand, there is much disagreement and confusion about the effects that these inductances have on the distribution of fields and currents in and around bulk rails and armatures (distributed parameter features). There are also unresolved theoretical issues regarding the fundamental nature of the emfs induced by the motion of the armature. The present work offers a treatment of the major induced fields in railguns and their connection to many of the unusual erosion effects observed in railgun tests. The analytical results are illustrated with examples using COMSOL finite element models. Supporting data from our laboratory firing tests are also presented.

1.1 Time varying currents

Referring to Figure 1, at any instant in time, as the armature moves along the rails of a railgun, separated by distance h. The current, I, flows through the armature and rails and generates magnetic fields so the system acts as a rectangular inductance loop.

The emf generated in the circuit, (see Figure 1) according to the Faraday flux rule, is given by

$$\text{emf} = \oint E' \cdot dl = -d\Phi/dt \qquad (1)$$

where Φ (=LI) is the flux in the rail/armature and L is the loop inductance at time t.

Recall that Equation 1 applies more generally in that it includes motional emf, which is the emf induced in the armature by a Lorentz force on the charge carriers inside the armature. The net emf in the circuit is properly computed by adding the rate of flux swept out by the moving armature to the flux created by dI/dt in $d\Phi/dt$ [1].

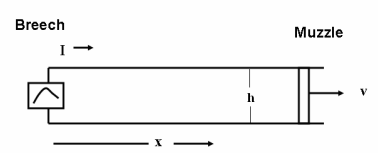

Figure 1. Railgun configuration with power supply at left delivering a current pulse which produces a magnetic field within the rails that drives the armature at velocity v.

Typical large test guns are 4 to 5 meters long, with rail separation, in the 3 to 4 cm range, and exit velocities in the 2 to 3 km/sec range. Typical peak currents in large systems are in excess of one million amperes.

Railgun rails also serve as long capacitor plates. These plates will acquire surface charges and surface currents in response to the power supply emf and the induced emfs. For dI/dt=0, there is no rail induction, and the power supply emf acts alone on the rails to produce a uniform surface charge and rail-to-rail potential along the railgun capacitor plates (neglecting the rail resistance for simplicity). For positive dI/dt, the resulting induced emf counters the power supply emf by acting to reduce the system current. For negative

dI/dt, the induced emf augments the power supply emf, by acting to increase the rail current. The above is as required by Lenz's law.

1.2 Armature motion

Again we refer to Figure 1. Recall the familiar physics textbook case where an external agent moves an armature through a uniform field B which creates an emf of magnitude Bvh. The present case (as we will describe in more detail later) is entirely different because, as the armature moves, the space behind the armature is continually filled with new flux. So we have true flux creation as the source of the emf from armature motion in railguns. Although its magnitude is given by Bvh, as in the motional emf case (B is the mean field created by the current I), there is no motional emf.

A more detailed treatment of emfs due to armature motion and time varying currents is offered in the following section.

2. Analysis

2.1 Induced emf from current changes

The seat of emf from dI/dt is uniformly distributed along the railgun conductors because E' is uniformly distributed. The electrostatic field E is the negative of the induced field E' within the seat of emf [2] (assuming negligible resistance). For the positive dI/dt case, the potential change along length x, in the top rail is –E'x and in the bottom rails it is +E'x; setting the sum of the potential differences to zero gives V_B-E'x-V(x)-E'x=0. (V_B is the potential across the breech end.) So the rail-to-rail potential for the initial positive dI/dt portion of the current pulse is

$$V(x) = V_B - 2E'x. \qquad (2)$$

In the case where the fields are generated by loop currents, Equation (2) can be rewritten using the total loop inductance, L, and the inductance per unit length, L_X. For large railgun length to height ratio, x_A /h, we obtain the net emf from the Faraday rule, $d\Phi/dt = 2E'x_A = LdI/dt = L_X x_A$ dI/dt. This gives E'= L_X dI/dt. From Equation 2,

$$V(x) = V_B - L_X x \, dI/dt. \qquad (3)$$

The rail-to-rail potential is reduced below the power supply potential everywhere along the rails.

For negative dI/dt portion of the current pulse, **E'** is directed along the current flow direction and the same expression holds. The rail-to-rail potential now is higher than the power supply potential everywhere along the rails.

At the peak value of the pulse, dI/dt=0 and V(x) = V_B all along the rails.

Taking the derivative of Equation (3) yields

$$dV/dx = - L_X \, dI/dt. \qquad (4)$$

This is essentially one of the two basic transmission line equations [1].

2.2 Induced emf from armature motion

Referring to Figure 2, in the laboratory frame, as the armature moves along the rails, in time interval, Δt, a new segment of current carrying rail is created which, in turn, creates a localized field, d**B**, as indicated. If the rail segment is approximated by a rod, then d**B** is given by the Biot and Savart inverse square expression for field creation.

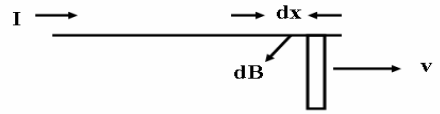

Figure 2. Illustration of mechanism of flux creation immediately behind the armature.

So, with armature motion, the induced emf exists in the immediate vicinity of the armature, so the full power supply voltage, V_B, appears along the entire length of the rails (neglecting the resistive term). In other words, the seat of emf resides primarily in the conducting surfaces (including the top and bottom rail sections) at the rear of the armature. This negative Bhv term is formed in the localized region, and thus provides a relatively sharp field and voltage reduction near the rear of the armature. Approximating the localized voltage reduction with the Heaviside function, H(x), we have,

$$V(x) = V_B - H(x - x_A)\, Bhv \qquad (5)$$

Equation (5) describes the condition where

$V(x) = V_B$ for $x < x_A$, and,

$V(x) = V_B - Bhv$ for $x > x_A$.

Equations (5) is the main consequence of the present theoretical treatment of the motion related emf in railguns.

3. COMSOL Models

A 2-D COMSOL model is used to check the validity of Equations 3-5. Electric field distributions are obtained for uniform flux creation from dI/dt and for concentrated flux creation associated with armature motion.

A 3-D axisymmetric model is used to illustrate the effects of flux creation at the rear of the armature on the time dependent current distributions within the body on an armature-like conductor. Our aim is to illustrate the basic physics, so simplified models are applied for convenience. It is not our intent to actually model the complex armature configuration

3.1 2-D model of electric fields

Figure 3 shows the 2-D model used to demonstrate the nature of the rail-to-rail electric fields generated by the positive dI/dt contribution, and by armature motion. The magnitudes of the applied currents are arbitrary, since the essential features are independent of actual magnitudes. The critical parameters are the armature conductivity, which was set at 1.9e7 S/m for the 7076-T6 aluminum alloy typically used in armatures; and the time frame of the simulation was set at 3 milliseconds to match typical railgun firing time durations. Copper parameters were used for the rails.

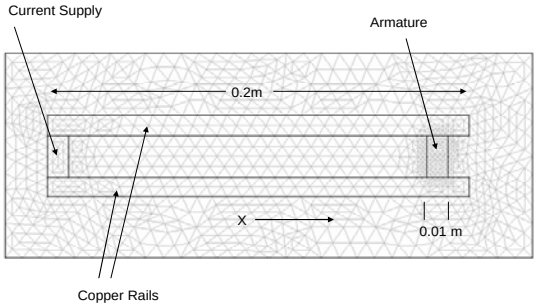

Figure 3. Model used to represent railgun configuration shown in Figure 1.

Transient solutions were generated. The applied current was set to increase linearly with time in the dI/dt example. The present approach to the emf caused by armature motion in terms of localized flux creation can be conveniently modeled using COMSOL. This is accomplished by setting the current to a constant value while the magnetization of a one centimeter domain within the rails at the rear of the armature was set to rise linearly with time.

Figure 4 gives the model results for the two cases.

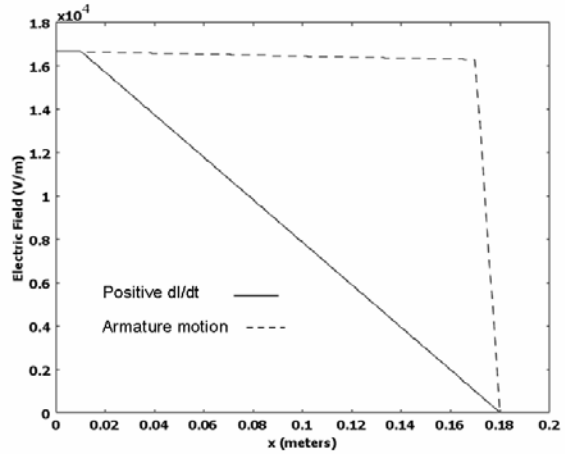

Figure 4. COMSOL model results showing railgun electric field distributions for uniform flux creation (dI/dt) and concentrated flux creation cases (armature motion).

The positive dI/dt inductance term produces a uniform, linear reduction in the rail-to rail electric field along the length of the rails in agreement with Equations (3) and (4). Localized flux creation, on the other hand, allows the high breech voltage to exist all along the rails. It is

only reduced in magnitude within the volume of localized flux creation.

3.2 3-D model of bulk diffusion effects

A 3-D model is used here for a more realistic description of the essential physics of field and current redistributions that arise from induced fields in railguns. A simplified 3-D model was generated in COMSOL using an axisymmetric ring of rectangular cross section. For our purposes, we consider that one half of the ring represents a standard C- shaped armature which generates a self-field, while the other half (dashed) contributes the field from the rails. The inset shows the assumed orientation of the ring between the rails. A similar approach is taken by Namias [4] to show that the fields at the armature are an equal mix of self-field and rail fields. Again, a 3 millisecond time duration was used to match typical railgun firing durations.

Figure 5 shows the 3-D axisymmetric ring configuration used in the model. The height z=4 cm and the radius r= 1 cm in this example. To simulate the effects of time varying currents during railgun firing, a current pulse (loop current) was applied to reproduce typical current vs. time distributions of railguns. The resulting system current initially rises to a peak at approximately 1 millisecond and drops off continuously beyond that time.

Resistive heating plots are shown along an axial cut through the ring. These plots reflect the current distributions within the volume of the armature for selected times in the positive and negative portions of the rail current pulse. The white areas indicate the locations of maximum heating and current density. Included are the arrow plot distributions of magnetic flux density through the armature volume for the two times. The positive dI/dt plot in Figure 5 shows the resistive heating distribution within the armature at 0.4 milliseconds (during the initial current rise). The increasing flux induces a back emf that acts primarily near the rear of the armature, and the induced current opposes the applied current at that location. The result is a reduction in net current at the rear of the armature, and a diversion of current and resistive heating to the top and bottom of the armature. The current concentrations are most intense at the back corners in this case.

The negative dI/dt plot shows the resistive heating result at 3.0 milliseconds (well beyond the current pulse peak). The currents diffuse towards the center in the negative dI/dt portion of the current plot. In this example, the merging of the two currents is complete at 3 milliseconds as indicated in this plot.

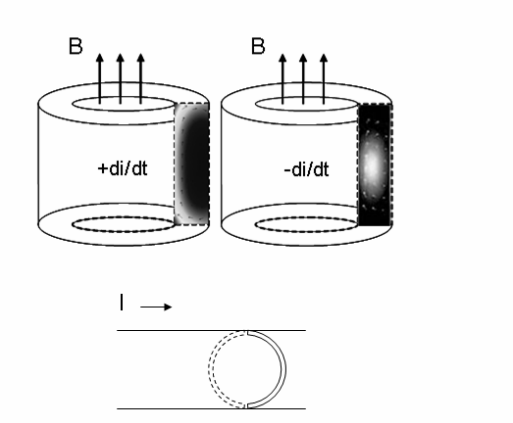

Figure 5. Model resistive heating plots showing effect of induced fields on current distributions within a circular armature section during positive and negative dI/dt portions of a current pulse. Diagram shows orientation of the ring between the armature rails.

The results shown here are generic in the sense that any conductors of these approximate dimensions and conductivities that are subjected to a similar pulse of current will experience similar induced emfs and similar current distributions. These COMSOL results reflect fundamental behavior of currents in bulk conductors and are not peculiar to railguns. In other words, one always expects currents to be driven forward to the top and bottom of a loop during the initial positive dI/dt portion of the current pulse. During the negative dI/dt portion of the current pulse, one will tend to get a merging of the current into the center of the conductor if the armature is small enough. For armature dimensions beyond a few centimeters, merging of the currents may not be possible because there is insufficient time for diffusion. It will be shown in the discussion section that these results offer an explanation formation of initial current tracks at the top and bottom rail

edges and the merging of these current tracks into a central track at downbore locations.

4. Experimental

A small scale launcher was developed for the purpose testing the validity of the analysis and COMSOL model results presented here. Power is supplied by switched capacitive energy sources, each coupled with a pulse shaping and current limiting inductance. It is comprised of 4 banks of 20, 3500mF electrolytic capacitors, with each bank coupled to a 10mH inductor. The capacitor banks are sequentially discharged in a controlled fashion in order to produce the desired current profile. In this study, we stage the banks to investigate the effect of dI/dt on the current distribution.

Aluminum rail liners were applied against the base copper rails. The system is designed to allow study of the progress of the localized currents across the rail surface at the armature/rail interface as the armature moves downbore. These localized current locations are recorded as melt tracks on the aluminum liner surfaces.

Pickup coils located at the center of each power supply inductor provide a means of measuring the current using the mutual inductance with the surrounding coil. The staging sequence is optimized to minimize pickup from the inductors of the other banks. The launcher is one meter in length with a 2.54 cm x 1.72 cm rectangular bore. The rails are held in position with G10 insulators.

Static firing experiments were also conducted on a 0.61 meter launcher railgun section using the subscale power supply. In these static experiments, an armature that is fixed in position at the muzzle is simulated using a copper muzzle shunt, while the power supply delivers the current pulse through the railgun. So, this configuration allows tests of our dI/dt analysis and of the COMSOL model results in the absence of a motion related emf. This technique allows application of potential probes all along the inner surfaces of the railgun to provide a direct measure of the rail-to-rail potential distributions from breech to muzzle during all phases of the current pulse. In the present test, potential probes were applied at 0.13m, 0.25m, 0.38m, 0.51m, and 0.61m. The objective here was to verify Equation (6) and the transmission line equation (Equation (7)).

4.1 Experimental Results and Discussion

Figure 6 are typical subscale firing test results. The figure shows a set of melt tracks comprising molten aluminum deposited on the aluminum rail surface. These melt tracks provide a record of the path taken by localized, concentrated currents that always form at the interface between the armature and rail in our tests.

The results are representative of dozens of similar test results. The most significant and reproducible features are the uniform, symmetric merging of the initially parallel pair of tracks into a single, central, downbore track and the highly concentrated nature of each individual track.

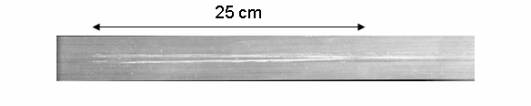

Figure 6. Molten armature tracks showing merger of initially parallel traces into a single, central trace.

Figure 7 shows the 1 x 2 x 4 cm armature after firing. The top and bottom edges are tapered in this experiment to control the area of contact. The eroded surface clearly shows a concentration of erosion in the central region of the armature face that is in contact with the rail surface. Typical eroded depths in the central eroded pit are in the 130 micron range. The maximum eroded depth was 164 microns. Optical microscopy shows heavy melting at the bottom of the eroded pit so that the erosion process is melting. The central location of the eroded pit coincides with the location of the central track that forms downbore on the rail surface during the negative dI/dt portion of the railgun current pulse (Figure 6). This is taken as direct evidence for current concentration in the center of conductors during the negative dI/dt portion of the current pulse, as predicted by the COMSOL model (Figure 5).

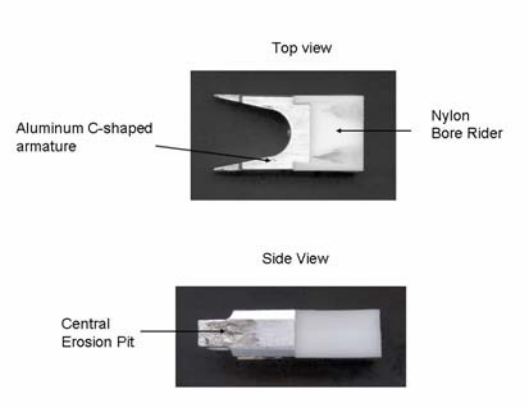

Figure 7. Armature after firing, showing maximum erosion location at a central region along the armature / rail interface.

Figure 8, shows results from our static firing experiments and compares the breech voltage readings and the readings at the 0.51 meter location, which is near the muzzle end of this railgun section. The railgun current pulse trace is also shown. As predicted by Equation 6 and the transmission line equation (Equation 7), the breech voltage exceeds the muzzle voltage during the positive dI/dt portion of the current trace; for the negative dI/dt portion of the current trace, the voltage near the muzzle exceeds the breech voltage, as predicted.

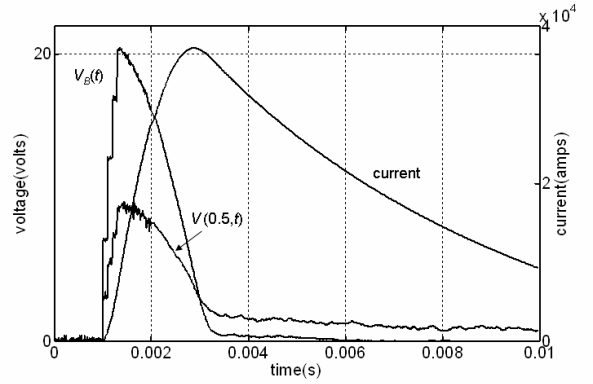

Figure 8. Static test results showing potential v. time data at the breech and at the 0.51m location. Railgun current is also shown.

Figure 9 compares the measured dV/dx with the predicted value from the transmission line equation (Equation (7). The experimental dV/dx values represent an average of five measured differences in voltage between the breech and each test location for each time increment. There are no fitting parameters for the theoretical plot; we used the measured value for Lx and the values of I and dI/dt needed for the equation were obtained from a polynomial fit through the measured time dependence of I. The agreement is remarkable, clearly verifying the validity of Equations (3) and (4).

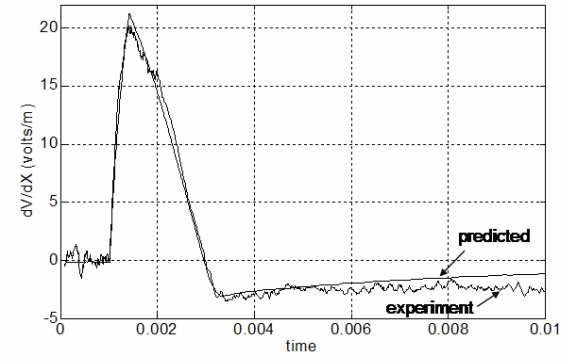

Figure 9. Comparison of measured dV/dx with the values predicted by Equations (3) and (4).

5. Railgun erosion

It is well known that rail surface erosion follows the pattern similar to that we observe in Figure 6. In larger high current systems, the concentrated currents are sufficient high to melt and erode the copper rail surfaces.

Another source of rail damage is the transition from molten armature interface conduction to a higher temperature plasma brush interface which characterized by generalized damage on the rail surfaces. Drobyshevski et al [4] associate this transition with the merging of the pair of current tracks into a single downbore track because the increased tendency for pinch instability at higher currents.

The present results provide a simple explanation for the presence and the behavior of the concentrated current tracks. An understanding of the phenomena associated with current concentrations can be useful in designing more erosion resistant armatures and rails.

6. Motion related emf

There is little consensus on the basic physics associated with armature motion and the emf that it generates. Namias [3] treats this in terms of motional emf , i.e., the motion of a conductor through a magnetic field. Delellis et al [5], on the other hand argue that the emf is generated by a combination of flux creation and motional emf. As a third example, Zahn [6] addresses this purely in terms of flux creation. In this paper we suggest a resolution to these conflicting views in terms of localized flux creation.

7. Invalid methods of analysis

Feynman et al [1] warn of the tendency for misapplications of the Faraday rule. We have experienced this in numerous private communications where invalid analyses of the problems we address here produced radically different results from our equations. This, in part, motivated our experiments whose results are shown in Figure 9. It seems to us that a major contributing factor for such common misapplications is the presence of erroneous methods of analysis in well-known textbooks. We find that COMSOL can be effective in helping to avoid these pitfalls.

8. References

1. R. Feynman, R. Leighton, and M. Sands, *The Feynman Lectures in Physics vol II*, Addison Wesley, Reading MA (1964).

2. J.R. Reitz and F.J. Milford, "*Foundations of Electromagnetic Theory*", Second Edition, Addison-Wesley Publishing Company, Reading MA (1967).

3. V. Namias, "Induced current effects in Faraday's law and introduction to flux compression theories" Am. J. Phys. **54** (1) (1986) 57-69.

4. E.M. Drobyshevski, R.O. Kurakin, S.I. Rozov, B. G. Zhukov, M.V. Beloborodyy, and V.G. Latypov, "The importance of three dimensions in the study of solid armature transition in railguns", J. Phys. D: Appl. Phys. **32**, (1999) 2910-2917.

5. R. Delellis, H. Kelly, and A. Marquez, "On the electromotive force in moving conductors", Am. J. Phys. **58** (11) (1980) 1064-1065.

6. M. Zahn, "*Electromagnetic Field Theory*", John Wiley &Sons, Inc. NY, 1979.